

EB-Net to landmark anatomical images

Le Van Linh^{a,c,*}, Beurton-Aimar Marie^{a,1}, Zemmari Akka^a, Parisey Nicolas^{b,1}

^a*University of Bordeaux, 351, cours de la Libération, 33405 Talence, France*

^b*UMR 1349 IGEPP, BP 35327, 35653 Le Rheu, France*

^c*Dalat University, Dalat, Lamdong, Vietnam*

Abstract

Deep learning has been introduced in the middle of the previous century for artificial intelligence program, and in recent years, it has risen strongly because of improvements in the computation performance. It has been applied to solve problems in different domains such as computer vision, speech recognition, or languages translation. Among different types of deep learning architectures, convolutional neural networks have been most often used in computer vision for image classification, object recognition, or key points detection and they have brought amazing achievements. In this work, we propose a new convolutional neural network model based on composition of elementary blocks of layers to predict key points (landmarks) on 2D anatomical biological images. Our proposed model has been trained and evaluated on a dataset including the images of 5 parts of 293 beetles. During the experiments, the network has been tested in two ways: training from scratch and applying fine-tuning process. The quality of predicted landmarks is evaluated by comparing the coordinates distance between predicted landmarks and manual ones which have been set by biologists. The final results have been provided to biologists and they have confirmed that

*Corresponding author

Email addresses: `van-linh.le@labri.fr` (Le Van Linh), `beurton@labri.fr` (Beurton-Aimar Marie), `zemmari@labri.fr` (Zemmari Akka), `nicolas.parisey@inra.fr` (Parisey Nicolas)

¹both authors contributed equally to this work.

the quality of predicted landmarks is statistically good enough to replace the manual landmarks for the different morphometry analysis.

Keywords: Deep learning, CNN, fine-tuning, landmarks

1. Introduction

In recent years, deep learning [1] is known as a solution for difficult tasks in different domains. It has been known as a part of machine learning domain. Computational model of deep learning is composed of multiple layers to learn data representation. Each layer extracts the representation of input data which comes from the previous layers, then it will compute a new output to the next layer. In a deep learning model, each layer may contain different number of nodes, called *neurons* which have been inspired from the biological neural system [2]. Currently, deep learning has many kinds of variant architectures and each of them has found success in such as: Deep Neural Network (DNN) to solve classification or data analysis problems[3, 4]; Convolutional Neural Network (CNN) in computer vision [5, 6, 7]; Recurrent Neural Network (RNN) on time sequences analysis [8, 9, 1, 10]. All of them have exhibited impressive performance comparing to more classical methods. In deep learning architectures, CNN is a specific network for pre-processing data which have grid topology, for examples, time series (1-D), 2D and 3D images, or video. From the first architecture [5] until now, many CNN models have been proposed and have succeeded in different tasks of computer vision such as image classification [5, 6, 7], object recognition [7, 11, 12], and key points detection [13, 14, 15, 16].

In computer vision, key points detection is an important field. In this field, algorithms try to find the key points (called points of interest (PoI) or landmarks) through images. The landmarks are considered as the points in the image that are invariant when the image changes e.g. by applying some morphological transformation. In biology, the landmarks are most often provided by

25 the biologists. Depending on the objective of work and the studied object, the number of landmarks may be different, as well as their position can be defined along the outline of the object or inside the object. From landmarks coordinates, it is possible to extract object characteristics and to apply measure, for examples, to detect human face [14], human pose [17] or topology of objects in
30 an organism in biology.

In this work, we propose a new composition of layers for a CNN architecture to predict the landmarks on biological species images. The proposed model has been trained on a dataset of 293 beetles images. We have also designed a specific procedure to augment our dataset because several hundred images are
35 usually considered as a modest number to apply deep learning methods. After applying our model, the biologists have asserted that the predicted landmarks which have been provided by our model, were enough good to replace the manual landmarks.

This paper is organized as followed: Section 2 discusses the related works
40 about deep learning and setting of landmarks on 2D images. Section 3 presents the method to augment our dataset. Section 4 explains the design of new network model. The first experiments of the network on each dataset are presented in Section 5. In the last section, we present a technique to improve the results of the proposed model: fine-tuning.

45 **2. Related works**

In the middle of the previous century, deep learning [1] have been introduced as a method for artificial intelligence applications. However, several problems appeared in order to take into account real-world cases because of the limitation of memory size or computing power. Nowadays, huge improvements of
50 computing capacities, both in memory size and in computing time with GPU

programming, have opened a new perspective for deep learning. In recent years, deep learning architectures have achieved remarkable accomplishments in many domains such as **computer vision** [5, 6, 7, 11, 12], **speech recognition** [4, 3], **language translation** [8, 9], **natural language processing** [1, 10, 18],

55 In computer vision, deep learning, specifically with CNN, has been used to achieve difficult tasks in image analysis such as image classification, objects or key points detection.

2.1. Overview of Convolutional Neural Network

A CNN is a feedforward network which takes the information following one
60 direction from the inputs to the outputs. Currently, CNNs have many variations, but in general, it consists of several types of layers: convolutional and pooling layers which are stacked together to convolve and to down-sample the inputs. Then, they are followed by one or more fully connected layers to achieve the output of the network from the application of a decision function.

65 Fig. 1 shows a classical example of a CNN, the network inputs directly an image to several stages of convolutional and pooling layers. Then, the representation is feed into three fully connected layers. A dropout layer is inserted after the second fully connected layer (it is represented by some blue nodes). Finally, the last fully connected layer gives the category label for the input image. This
70 architecture could be seen as the most popular one. Now, we will describe the different types of layers, readers familiar to tem can jump directly to the next section.

Convolutional (CONV) layer is used as a feature extractor by applying some learnable weights (filters) on the input images. The input image is convolved
75 with the filters in order to compute the new feature maps; then, the convolved results are sent through a nonlinear activation before sending to the next layer. In CONV layer, the neurons are arranged into feature maps. All the neurons

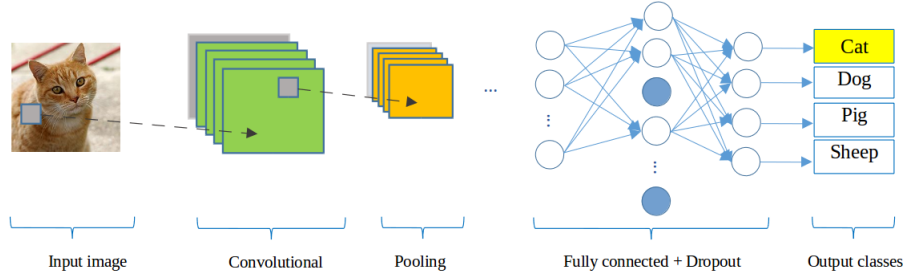


Figure 1: A CNN network for classification problem

within a feature map have the same constraints; however, different features maps within the same CONV layer have different weights so that several features can
80 be extracted at each location of an input image.

Pooling (POOL) layer is mostly used to down-sampling the size of the input with the purpose to reduce the spatial resolution of the feature map and so to reduce the computation cost. Initially, it was a common practice to use average pooling to propagate the average of all the inputs to the next layer. However, in
85 more recent models [6, 19, 12], maximum pooling function has been preferred. It propagates the maximum values of the inputs to the next one. Fig. 2 illustrates the differences between maximum and average pooling: Giving an input image of size (4×4) , if applying a filter with size of (2×2) and a stride of 2, if we apply to the yellow region an average pooling, the output will be 36.25 and a
90 maximum pooling will return the value 122.

Dropout (DROP) [20] is a technique used to prevent the over-fitting during the training. The term dropout mentions dropping some output units and their connections (incoming and outgoing) belonging to a layer in the network. The units are dropped randomly with a probability p . When applying dropout tech-
95 nique, the network becomes a collection of thinned networks [20]. So, training a neural network with dropout looks like training a collection of thinned networks. The dropouts layers are most often placed after the fully connected layers, but

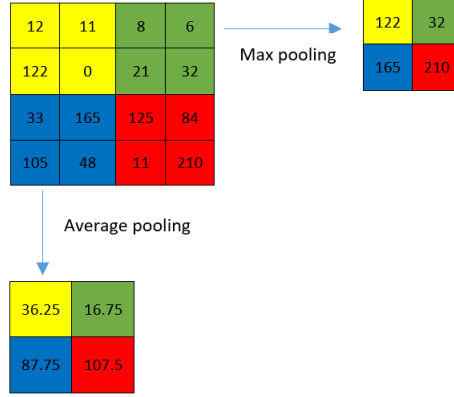


Figure 2: The results of different pooling

it is possible to use them after the pooling layers to introduce some kind of images noise augmentation.

100 Fully connected (FC) layer usually follows the group of convolutional and pooling layers to extract the abstract feature representations of the image. A CNN may have one or several FC layers. They interpret the feature representations (their inputs) and perform a function of high-level reasoning by applying the activation functions. In practice, the last fully connected layer produces
 105 the output of the network and choosing the activation function is depended on which kind of problem that network solves.

2.2. State of the arts in deep learning and key points detection

LeNet [5] model is considered as the first architecture of CNN. LeCun et al. [5] have used LeNet to classify the handwritten digits in cheques. LeNet
 110 exhibits a standard architecture of a CNN which consists of convolutional layers, pooling layers, followed by two fully connected layers. But to be applied to realistic problems, this model requires huge computation capacities and a large amount of training data which are not available at the early 2000s. In the last ten years, as the capabilities to compute have been drastically improved and in

115 the same time, a huge amount of data became available, new models of neural
networks appear well adapted to this new environment. One of the first ones is
AlexNet [6], which is similar to LeNet [5] but with a deeper structure: LeNet has
2 convolutional layers and 1 fully connected layer while AlexNet has 5 and 3, re-
spectively. Furthermore, in AlexNet the activation functions have been changed
120 and dropout layers have been added to prevent the over-fitting. AlexNet won
the famous ImageNet Challenge² in 2012. From the success of AlexNet, a lot of
different models have been proposed to improve the performance of CNN, one
can cite ZFNet [21], GoogLeNet [7], VGGNet [22], or ResNet-50 [23]. The main
difference between these networks is that their architectures became deeper and
125 deeper by adding more layers, e.g. ResNet-50, which won the champion of
ILSVRC 2015, is deeper than AlexNet around 20 times.

Besides classification or recognition of objects, CNNs have been also used
to detect key points inside images. Liu et al. [13] have presented a method
to predict the positions of functional key points on fashion items such as the
130 corners of neckline, hemline and cuff. Yi Sun et al. [14] have proposed a CNNs
cascade to predict the facial points on the human face. Their model contains
several CNNs which are linked together in a list as a cascade. Three levels of
the cascade are set to recognize the human face from the global to local view
with the objective to increase the accuracy of predicted key points. In the same
135 topic, Zhanpeng Zhang et al. [15] have proposed a *Tasks-Constrained Deep
Convolutional Network* to join facial landmarks detection problem with a set of
related tasks, e.g. head pose estimation, gender classification, age prediction,
or facial attribute inference. In their method, the input features have been
extracted by 4 convolutional layers, 3 pooling layers and 1 fully connected layer
140 which is shared by multiple tasks in the estimation step. Shaoli Huang et al. [17]

²This is a challenge where evaluates algorithms for object detection and image classification.

have introduced a coarse-fine network to locate keypoints and to estimate human poses. Their framework consists of the base convolutional layers shared by two streams of keypoint detectors: The first stream, named coarse stream, includes 3 detector branches (3 stacks of Inception modules [7]) which are used to focus
145 on capturing local characteristics and modeling spatial dependencies between human parts. The second one, named fine stream, receives features which are concatenated from the coarse stream and provides the accurate localization. Cintas et al. [16] have introduced an architecture which is enable to recognize
45 landmarks on human ears. Their proposed model includes a structure with
150 2 convolutional layers, 1 pooling layers, and 1 dropout layer to extract the features. This structure is repeated 3 times and is followed by 3 fully connected layers. In the same context of key point detection, we have developed a CNN to automatize landmarks prediction on beetle’s anatomies.

From AlexNet period to ResNet-50, the obtained success stories [6, 23] have
155 proved that CNN models produce better results on a large dataset. To use this technique, the size of dataset remains as a bottleneck. The next section is turn to the description of the method we have designed to augment the size of the dataset.

3. Data augmentation

160 The fundamentals of deep learning algorithms are to train the models on dataset repeatedly in order to reach the best accuracy. So, providing a large dataset asserts to learn more cases and clearly improves the learnable of the network. Unfortunately, in some application domains as in biology, providing large dataset is costly and could be difficult to obtain. For this reason, one way
165 to solve this problem is to create misshapen data from real data and to add them to the training set. Most often in image processing, dataset augmentation

uses operations like translation, rotation or scaling which are well known to be efficient to generate new version of existing images. However, this kind of operations are not useful in our case because the analysis of images by CNN (convoluted) are most often invariant to translation or rotation. So, we have designed another method to obtain misshapen images.

Our image set is in RGB color map, the first procedure consists of changing the value of one color channel of the three channels in the original image to generate a new image. A constant value is sampled in an uniform distribution $\in [1, N]$ to obtain a new value capped at 255. For example, Fig. 3 shows the three images which are generated when a constant $c = 10$ is added to each channel of an original image. Following this way, we can generate three new versions of only one image.

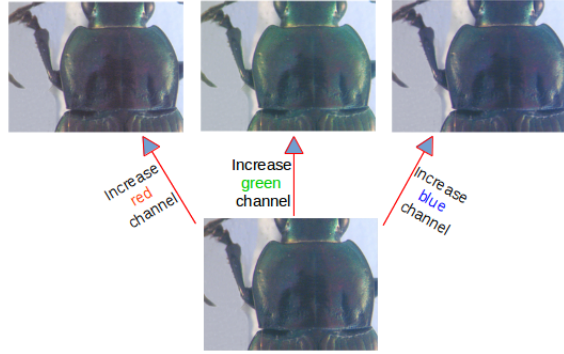


Figure 3: A constant $c = 10$ has been added to each channel of an original image

In the second procedure, each channel is considered separately and one gray image is generated for it (Fig. 4). Consequently, we obtain 3 new images (single channel) from an original one. At the end of the process, 6 versions of an original image are made. In total, the new data set contains $293 \times 7 = 2051$ images for each anatomical part of beetle (an original image and six misshapen ones).

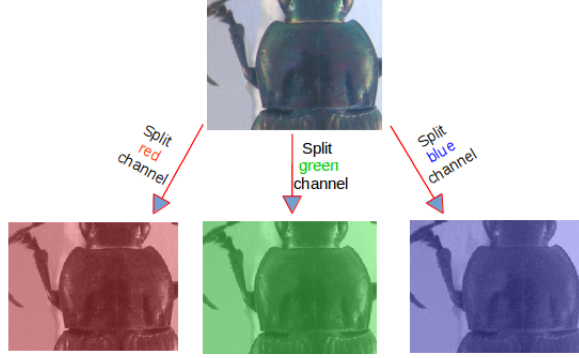


Figure 4: Three channels (red, green, blue) are separated from original image

4. Network architectures designing

As we have presented previously, several CNN architectures are available from literature and tools libraries. It is always possible to adapt them to a specific application by changing the parameters values or by modifying the arrangement of layers. By the way, several trials have been achieved before to obtain a satisfying model dedicated to landmarks estimation. In this section, we present three versions of the model that we have designed to solve this task. As usual, we have combined the classical layer types to build the model, i.e., convolutional, maximum pooling, dropout, and full-connected layers.

The first architecture has been a very classical one (Fig. 5). It receives an input image with the size of $(1 \times 192 \times 256)$, then it is composed by three repeated structures of a convolutional (CONV) layer followed by a maximum pooling (POOL) one. In most of CNNs, the parameters of CONV layers have been set to increase the depth of the images from the first to the last layer. This is done by setting the number of filters at each CONV layer. In this first model, the depths of the CONV layers increase from 32, 64, to 128 and with different size of the kernels: (3×3) , (2×2) and (2×2) , respectively. Inserting POOL layers after a convolutional layers is usually done. The POOL layer

effects to progressively reduce the spatial size of the representation to reduce the number of parameters, computation in the network, and also to control over-fitting. The operation of POOL layers is independent for each depth slice of their inputs. In our model, we have used the most common form for one POOL layer: a filter with size of (2×2) and a stride of 2 pixels. At the end of the model, three FC layers have been added to extract the global relationship between the features and to proceed the outputs. The first two FC layers have been applied the activation functions to make sure these nodes interact well and to take into account all possible dependencies at the feature level. The outputs of the FC layers are 500, 500 and 16. The output of the last FC layer corresponds to the coordinates (x and y) of 8 landmarks which we would like to predict. Nevertheless, the obtained results with this architecture has not been considered as enough good to continue to use it. One of the main problems is the presence of over-fitting during the training process (Detailed results will be discussed in Section 5).

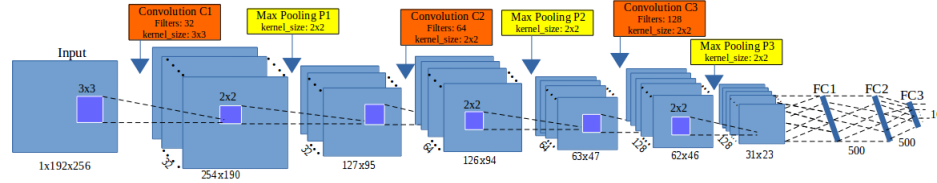


Figure 5: The architecture of the first model

The second model has kept the same architecture but the number of output of the two FC layers has been increased to 1000. Increasing the value at FC layers could allow to get more features from CONV layer without requirements of computing resources. However, the obtained results remained not satisfying, it will be discussed in the result section (Section 5).

To build the third architecture, we have defined a new concept: the *elementary block*. An elementary block is defined as a sequence of a CONV (C_i), a

maximum POOL (P_i) and a dropout (D_i) layers (Fig. 6). The Dropout layer
 225 has been added to prevent over-fitting by addition of a step of removal of some
 nodes. This significantly reduces overfitting and gives major improvements over
 other regularization methods [20]. The final architecture is a composition of
 elementary blocks.

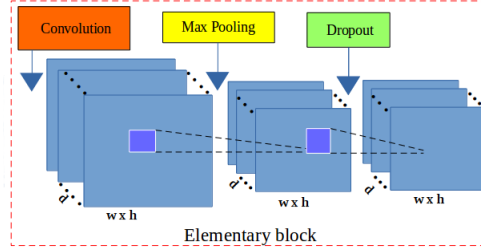


Figure 6: The layers in an elementary block. It includes a CONV layer (red), a maximum
 POOL layer (yellow) and a DROP layer (green).

Fig. 7 illustrates the layers in the third architecture. For our purpose, we
 230 have assembled **3 elementary blocks**, the main components of **EB-Net**. The
 parameters for each layer in each elementary block are described as below, the
 list of values follows the order of elementary blocks ($i = [1..3]$):

- CONV layers:
 - Number of filters: 32, 64, and 128
 - Kernel filter sizes: (3×3) , (2×2) , and (2×2)
 - Stride values: 1, 1, and 1
 - No padding is used for CONV layers
- POOL layers:
 - Kernel filter sizes: (2×2) , (2×2) , and (2×2)
 - Stride values: 2, 2, and 2
 - No padding is used for POOL layers

- DROP layers:
 - Probabilites: 0.1, 0.2, and 0.3

Three FC layers are kept the same as the second architecture: FC1 and FC2 have 1000 outputs, the last FC layer (FC3) has 16 outputs. As usual, a dropout layer is inserted between FC1 and FC2 with a probability equal to 0.5.

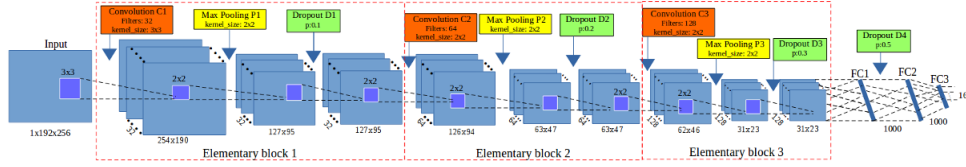


Figure 7: The architecture of EB-Net

The core of CNN is training over iteration. There are many ways to optimize the learning algorithm, but gradient descent [24] is currently a good choice to reduce the loss in neural network. The core idea is to follow the gradient until to reach stable state. So, we have chosen gradient descent in the backward phase to update the values of learnable parameters and to increase the accuracy of the network. The networks are designed to use the same learning rate and a momentum. The learning rate is initialized at 0.03 and stopped at 0.00001, while the momentum is updated from 0.9 to 0.9999. Their values are updated over training time to fit with the number of epochs ³ by applying parameters adjustment during the training. The three architectures implementations have been done on Lasagne framework [25] by Python code. More information about the model can be obtained from the repository on GitHub: https://github.com/linhle vandlu/CNN_Beetles_Landmarks

³An epoch is a single pass through the full training set

260 5. Experiments and results

This work is a part of a project about automatized morphology. The choice to turn to deep learning process has been motivated by the high difficulty to segment some parts of the beetle images and consequently to apply classical image processing methods. The pronotum was the first part we have analyzed with deep learning. The networks have been trained in 5,000 epochs on Linux OS by using NVIDIA TITAN X cards. During the training, the images are chosen randomly from the dataset with a ratio of 60% for training and 40% for validation. For each image, a set of 8 manual landmarks are available. They have been set by biologists and are considered as the ground truth for the evaluation.

265 In deep learning, many kinds of loss expressions can be considered depending on the class of problem solving by the network, for example, Root Mean Square Error (RMSE) is usually used for regression problems where the outputs are not discrete values. In the context of deep learning, landmark prediction can be seen as a regression problem because the coordinates of landmarks do not belong to discrete classes.

270 Therefore, RMSE has been used to compute the losses of architectures during the training process.

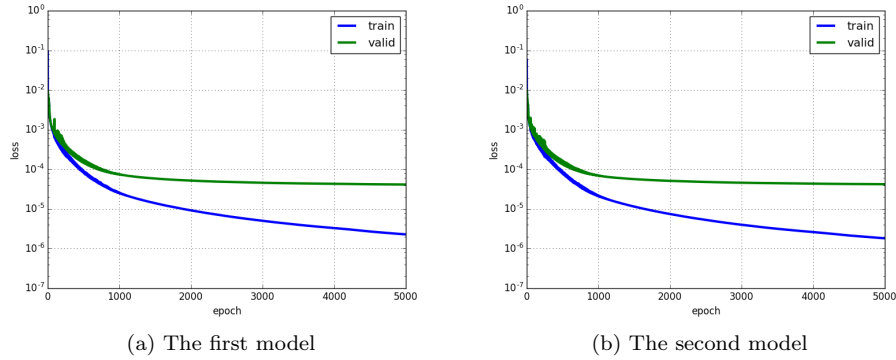


Figure 8: The losses (training and validation) of the models

Fig. 8a shows the training errors and the validation errors during training

phase of the first architecture. The blue curve presents the RMSE errors of training process while green curve is the validation errors. Clearly, over-fitting has appeared in the first model, i.e., training losses are able to decrease but validation losses are stable. In the second model (Section 4), the parameters of full-connected layers have been modified to prevent the over-fitting but it seems that this solution is still not satisfying, the results are very similar to the previous ones (over-fitting is still appears).

Fig. 9 illustrates the losses during the training of the third model, one can note that after several epochs, the two-loss values become closed and the over-fitting disappears. The sequence of Dropout addition inside elementary block works well to prevent over-fitting and improve the accuracy of the model greatly. This third model has been selected to compute automatically landmarks.

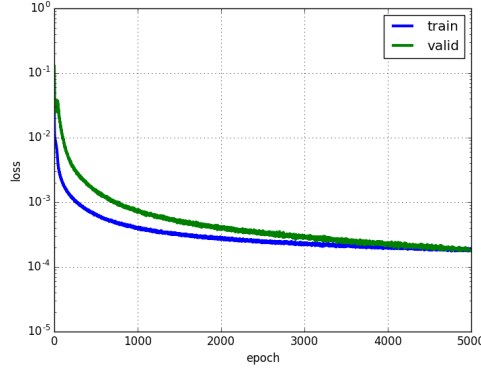


Figure 9: The losses (training and validation) of the third model

In order to extract predicted landmarks from all pronotum images, we have applied *cross-validation* procedure to choose the test images, we call it *round*. For each round, we have decided to choose 33 images for testing step. In order to predict landmarks for all available images, we will do 9 rounds. The remaining images are used as training and validation images. Of course, this dataset will be augmented as described before to provide 1820 images for these

2 steps. Table. 1 resumes the losses of 9 rounds when we trained the third model on pronotum images. Clearly, the training/validation loss among rounds are tiny and stable.

Round	Training loss	Validation loss
1	0.00018	0.00019
2	0.00019	0.00021
3	0.00019	0.00026
4	0.00021	0.00029
5	0.00021	0.00029
6	0.00019	0.00018
7	0.00018	0.00018
8	0.00018	0.00021
9	0.00020	0.00027

Table 1: The losses during training the third model on pronotum images

To evaluate the coordinates of predicted landmarks, the correlation metrics
 300 between the manual landmarks and corresponding predicted ones have been
 computed. Table. 2 shows the correlation scores of 3 metrics (using *scikit-learn* [26]), e.g. coefficient of determination (r^2), explained variance (EV), and
 Pearson correlation. These three metrics are both appropriate for our dataset
 type. The results closed to 1 show that the predicted coordinates are very
 305 close with the ground truth. It proves that our prediction is good enough
 to replace manual landmarks in statistical analysis of pronotum morphology.
 However, standing on the side of image processing, seeing the real coordinates on
 images is more appropriate than statistical results. So, the distances (in pixels)
 between manual coordinates and predicted coordinates have been calculated for
 310 all images. Then, the average distance for each landmark has been computed.

Metric	r^2	EV	Pearson
Score	0.9952	0.9951	0.9974

Table 2: Correlation scores between manual landmarks and predicted landmarks

Table. 3 shows the average distances by landmarks on all images of pronotum dataset. With the images resolution 256×192 , we can consider that an error of 1% (corresponding to 2 pixels) could be an acceptable error. Unhappily, our results exhibit average distance of 4 pixels in the best case, landmark 1 and
 315 more than 5 pixels in the worse case, landmark 6.

Landmark	Distance (in pixels)
1	4.002
2	4.4831
3	4.2959
4	4.3865
5	4.2925
6	5.3631
7	4.636
8	4.9363

Table 3: The average distances on all images per landmark on pronotum images.

Fig. 10 shows the distribution of the distances on the first landmark of all images. The accuracy based on the distance in each image can be separated into three spaces: best results, the images having distance less than the average value (4 pixels): 56.66%; acceptable results, the images having the distance from
 320 the average value to 7 pixels (standard deviation error): 31.40%; and the images which are clearly in error with the distance greater than 7 pixels: 11.94%.

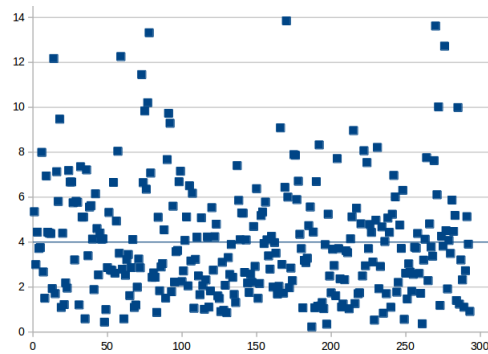


Figure 10: The distribution of the distances on the first landmark. The blue line is the average value of all distances.

To illustrate this purpose, Fig. 11 shows the predicted landmarks on two test images. One can note that even some predicted landmarks (Fig. 11a) are closed to the manual ones, in some case (Fig. 11b) the predicted ones are far from the expected results. So, the next step has been dedicated to the improvement of these results.

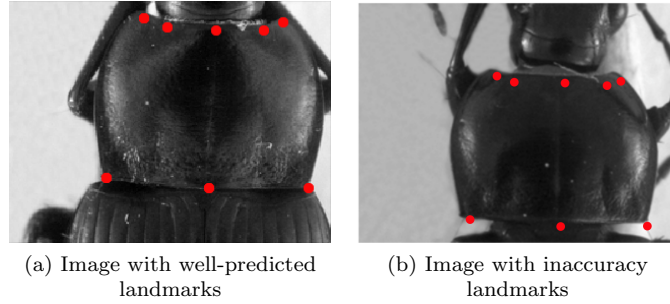


Figure 11: The predicted landmarks, in red, on the images in test set.

6. Resulting improvement by fine-tuning

EB-Net, which was presented in Section 4, have been trained from scratch on five datasets of beetles (left mandible, right mandible, pronotum, elytra, and head). At that step, the network was able to predict the landmarks on the images. But as we have discussed, even if the strength of the correlation seems to validate the results, when we display the predicted landmarks on the images, the quality of the predicted coordinates are not enough precise, and the average distances are a little bit high.

Training a network from scratch is not the only way to work in Deep learning. It is possible to initialize parameter values with values extract from another experiment on another dataset. It is called transfer learning [27]. Transfer learning aims to address the problem when the distribution of the training data from the source domain is different from that of the future data from the target

domain [28]. In order to improve our results, we have broadened model with this technique. In the idea, the obtained parameters values of a model, which have been used to solve a problem, are reused on other datasets [29]. The name of this procedure is currently called **fine-tuning**.

Fine-tuning does not only replace and retrain the last layer of the model on the new dataset but also fine-tunes the weights of a trained model by continuing the backpropagation. In deep learning domain, ImageNet [30] is a well-known dataset with more than 100,000 images. It has been used to train many famous CNN architectures such as AlexNet [6], VGG-16 [22], which have achieved the large success. The pre-trained models on ImageNet then have been shared in deep learning community as a source for the researcher who would like to continue using the features of ImageNet. Unfortunately, some preliminary tests have shown that re-using ImageNet features is not relevant for our application because landmarks detection has a difference from image recognition. On the other hand, we noticed that our problem is related to face recognition and facial keypoints detection. So, we have decided to train our model on a facial keypoints dataset which is considered as a source domain. Then, the trained parameters are transferred to predict landmarks on beetle’s images as target domain.

6.1. Pre-train model architecture with facial keypoints dataset

Facial keypoints dataset has been published on Kaggle community ⁴ by University of Montreal. It includes 2,140 human face images with the size of 96×96 . Each image contains 15 landmarks on the face: 6 landmarks for eyes, 4 landmarks for eyebrows, 4 landmarks for mouth, and 1 landmarks for nose tip. Fig. 12 shows four face images in the dataset and the landmarks on each the face.

⁴<https://www.kaggle.com/c/facial-keypoints-detection>

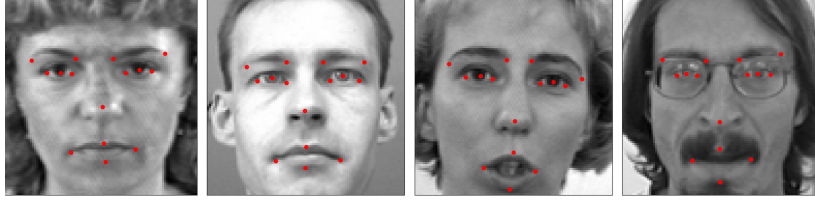


Figure 12: Four face images in the dataset and ground truth position of the landmarks.

365 For the pre-training step, EB-Net continues to be selected to train the facial
keypoint dataset instead of using other models. The objective of this task is
to evaluate and to compare the effectiveness of EB-Net and other promotions
in the challenge. Basically, the architecture parameters (number filters, size of
filter, padding, stride) are the same as working on beetle’s parts. We have just
370 changed the input size of network model to 96×96 and the output of the last
FC layers to correspond to the number of landmarks (15 landmark). For hyper-
parameters of model, the learning rate and momentum have been remained the
same. However, the number of epochs have been changed to 10,000 instead of
5,000 to achieve better learning on the parameters. After training, the RMSE⁵
375 score that obtained is 1.1464. This score is better than top 3 on the leader
board of challenge. It proved that EB-Net fits perfectly with facial keypoints
challenge and we have good reason to believe that the obtained parameter values
of EB-Net on facial keypoints dataset can use to fine-tune on beetle’s images.

6.2. Fine-tuning on each beetle’s part

380 EB-Net has been pre-trained on facial keypoints dataset with 30 outputs
(15 landmarks). Then, the parameters have been transfered to fine-tune on the
images of each beetle’s part. The fine-tuning stage has been done by continuing
the backpropagation to update the layers parameters.

⁵RMSE: Root Mean Square Error

In another scene, to be able to use the same parameters for fine-tuning
 385 process, the input images have been cropped to suppress the part which are
 empty, to obtain a new image size of 192×192 ; and a modification was made
 on stride properties of the first convolutional layer (changing from 1 to 2).

During fine-tuning, cross-validation has been applied to select data for train-
 ing and validation. After finishing the fine-tuning process, EB-Net was used to
 390 predict the landmarks on test images. To evaluated the accuracy of the model's
 output, the distances (in pixels) between predicted and corresponding man-
 ual landmarks have been calculated. Then, the average distances have been
 computed based on the distances. Tables. 4, 5, 6, 7, and 8 show the average
 distances by landmarks on each beetle's part of two processes: training from
 395 scratch and fine-tuning process. **From scratch** columns remind the previously
 average distances when EB-Net was trained from scratch. **Fine-tune** columns
 present the new average distances after applying fine-tuning on each part. The
 green and red values represent the best and the worst average distances on each
 part. From these tables, there is a difference in average distances between two
 400 process, the average distances of each landmark has decreased in the case of
 fine-tuning. It is clearly proved that the quality of predicted landmarks with
 the help of fine-tuning is more precise than training from scratch.

#LM	From scratch	Fine-tune
1	4.00	2.99
2	4.48	3.41
3	4.30	2.98
4	4.39	3.54
5	4.29	3.37
6	5.36	4.06
7	4.64	2.93
8	4.94	3.64

Table 4: Average distances comparison between training from scratch and fine-tuning on
 pronotum images

#LM	From scratch	Fine-tune
1	5.53	4.82
2	5.16	4.21
3	5.38	4.73
4	5.03	4.11
5	4.18	2.76
6	4.45	3.50
7	4.79	3.92
8	4.53	3.40
9	5.14	4.17
10	5.06	3.94

Table 5: Average distances comparison between training from scratch and fine-tuning on head images

#LM	From scratch	Fine-tune
1	3.87	3.21
2	3.97	3.28
3	3.92	3.20
4	3.87	3.22
5	4.02	3.31
6	4.84	4.21
7	5.21	4.54
8	5.47	4.76
9	5.27	4.55
10	4.07	3.39
11	3.99	3.29

Table 6: Average distances comparison between training from scratch and fine-tuning on elytra images

#LM	From scratch	Fine-tune
1	9.13	5.28
2	6.72	4.05
3	6.87	4.01
4	6.77	4.02
5	7.13	3.92
6	6.94	3.88
7	7.32	4.01
8	7.41	4.16
9	7.58	4.35
10	7.63	4.46
11	7.69	4.72
12	8.42	5.08
13	7.99	4.50
14	7.49	4.26
15	7.79	4.62
16	8.52	6.04

Table 7: Average distances comparison between training from scratch and fine-tuning on left mandible images

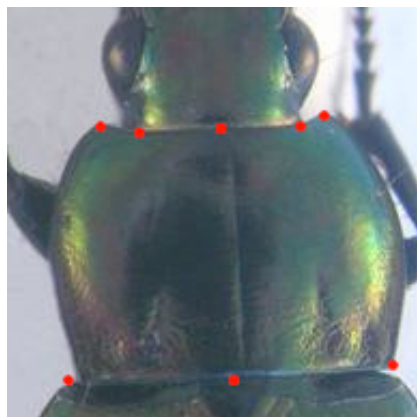
#LM	From scratch	Fine-tune
1	9.50	4.86
2	7.17	4.06
3	7.24	3.97
4	7.04	3.87
5	7.16	4.05
6	7.57	3.82
7	7.43	3.77
8	7.66	3.87
9	7.79	3.96
10	8.02	3.97
11	8.31	4.27
12	8.16	4.42
13	8.89	4.87
14	9.18	4.93
15	8.79	4.46
16	8.31	4.17
17	8.29	4.57
18	8.89	5.89

Table 8: Average distances comparison between training from scratch and fine-tuning on left mandible images

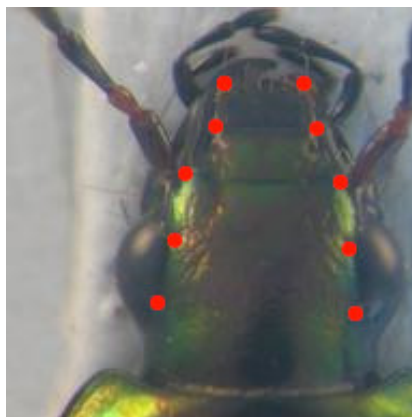
In order to get a better view about predicted landmarks, we have calculated other statistical indicators such as median, standard error, minimum value and maximum value on each landmark based on the distances between predicted and corresponding manual landmarks. All statistical values and the distribution graphs are presented in Appendix A. From these tables, the minimum and the maximum distances have a large difference in all cases. However, the median values, which separate the set into two parts, are very close with minimum values and so far from maximum values, even smaller than the mean distances. It confirms that almost distances stay around the median values and the predicted landmarks are good enough to replace the manual ones. Besides, the distribution of the distances on each landmark of each part have been taken into account in Appendix B. We can observe that most of distances are close with the mean and median values, only some exceptional cases. Fig. 13 shows the predicted landmarks of fine-tuning process in one case of each part.

The fine-tuning process has improved the results of the proposed architecture on both 5 datasets: left, right mandible, pronotum, elytra and head. All the average distances have significantly decreased: $\approx 41.35\%$ on left mandible, $\approx 46.51\%$ on right mandible, $\approx 25.98\%$ on pronotum, $\approx 15.8\%$ on elytra, and $\approx 18.10\%$ on head part based on considering the average distances per landmark. Besides, if we consider a predicted point which has the distance (from manual ones) less than mean value plus standard deviation is acceptable, the accuracy of method on each part is **87.07%** on pronotum, **87.92%** on head, **91.78%** on elytra, **93.58%** on left mandible and **88.31%** on right mandible.

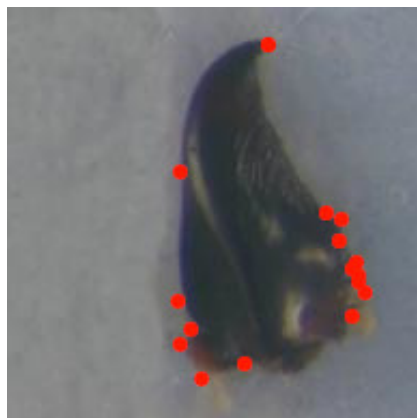
For segmentable images, we have a comparison between the results of deep learning and early method where we have applied image processing techniques to predict the landmarks [31]. Clearly, the result with fine-tuning has improved the location of estimated landmarks. Even the average distances which obtained



(a) Pronotum



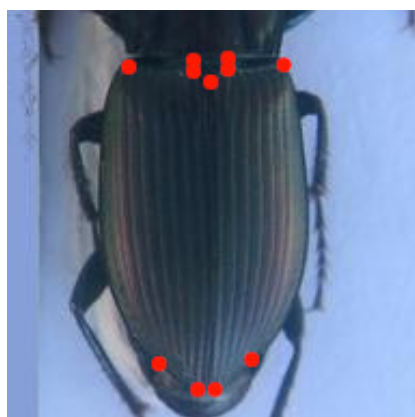
(b) Head



(c) Left mandible



(d) Right mandible



(e) Elytra

Figure 13: The location of predicted landmarks (red points) in one case of each part

430 from scratch training are still high but they are more stable than the results from
the early method: most of the average distance(or landmarks) of left mandibles
are less than the results of the early method, while the average distances are
very closed in the case of right mandibles.

7. Conclusion

435 In this work, we have presented how to apply convolutional neural network to
predict the landmark on 2D anatomical images of beetles. After going through
many trial models, we have presented a convolutional neural network for au-
tomatic detection landmarks on anatomical images of beetles which includes
the repeated of some elementary blocks (an elementary block consists of a con-
440 volutional layer, a max pooling layer, and a dropout layer) followed by fully
connected layers. Then, the proposed model have been trained and tested by
using two strategies: *train from scratch* and *fine-tuning*.

In our case, the size of dataset is limited. Therefore, we have applied the
image processing techniques to augment dataset. The predicted landmarks have
445 been evaluated by calculating the distance between manual landmarks and cor-
responding predicted landmarks. Then, the average of distance errors on each
landmarks has been considered.

The results have been shown that using the convolutional network to predict
the landmarks on biological images leads to satisfying results without need for
450 segmentation step on the object of interest. The best set of estimated landmarks
has been obtained after a step of fine-tuning using the whole set of images that
we have for the project, i.e. about all beetle parts. The quality of prediction
allows using automatic landmarking to replace the manual ones.

References

- 455 [1] Y. LeCun, Y. Bengio, G. Hinton, Deep learning, *Nature* 521 (7553) (2015) 436–444.
- [2] M. A. Arbib, *Brains, machines, and mathematics*, Springer Science & Business Media, 2012.
- [3] G. Hinton, et al., Deep neural networks for acoustic modeling in speech
460 recognition: The shared views of four research groups, *IEEE Signal Processing Magazine* 29 (6) (2012) 82–97.
- [4] T. Mikolov, et al., Strategies for training large scale neural network language models, in: *Automatic Speech Recognition and Understanding (ASRU)*, 2011 IEEE Workshop on, IEEE, 2011, pp. 196–201.
- 465 [5] Y. LeCun, L. Bottou, Y. Bengio, P. Haffner, Gradient-based learning applied to document recognition, *Proceedings of the IEEE* 86 (11) (1998) 2278–2324.
- [6] A. Krizhevsky, I. Sutskever, G. E. Hinton, Imagenet classification with deep convolutional neural networks, in: *Advances in neural information processing systems*, 2012, pp. 1097–1105.
- 470 [7] C. Szegedy, et al., Going deeper with convolutions, *Cvpr*, 2015.
- [8] S. Jean, K. Cho, R. Memisevic, Y. Bengio, On using very large target vocabulary for neural machine translation, *arXiv preprint arXiv:1412.2007*.
- [9] I. Sutskever, O. Vinyals, Q. V. Le, Sequence to sequence learning with
475 neural networks, in: *Advances in neural information processing systems*, 2014, pp. 3104–3112.

- [10] R. Collobert, J. Weston, L. Bottou, M. Karlen, K. Kavukcuoglu, P. Kuksa, Natural language processing (almost) from scratch, *Journal of Machine Learning Research* 12 (Aug) (2011) 2493–2537.
- 480 [11] C. Farabet, C. Couprie, L. Najman, Y. LeCun, Learning hierarchical features for scene labeling, *IEEE transactions on pattern analysis and machine intelligence* 35 (8) (2013) 1915–1929.
- [12] H. Li, Z. Lin, X. Shen, J. Brandt, G. Hua, A convolutional neural network cascade for face detection, in: *Proceedings of the IEEE Conference on Computer Vision and Pattern Recognition*, 2015, pp. 5325–5334.
- 485 [13] Z. Liu, S. Yan, P. Luo, X. Wang, X. Tang, Fashion landmark detection in the wild, in: *European Conference on Computer Vision*, Springer, 2016, pp. 229–245.
- [14] Y. Sun, X. Wang, X. Tang, Deep convolutional network cascade for facial point detection, in: *Proceedings of the IEEE conference on computer vision and pattern recognition*, 2013, pp. 3476–3483.
- 490 [15] Z. Zhang, et al., Facial landmark detection by deep multi-task learning, in: *European Conference on Computer Vision*, Springer, 2014, pp. 94–108.
- [16] C. Cintas, et al., Automatic ear detection and feature extraction using geometric morphometrics and convolutional neural networks, *IET Biometrics* 6 (3) (2016) 211–223.
- 495 [17] S. Huang, M. Gong, D. Tao, A coarse-fine network for keypoint localization, in: *The IEEE International Conference on Computer Vision (ICCV)*, Vol. 2, 2017.
- 500 [18] R. Collobert, J. Weston, A unified architecture for natural language processing: Deep neural networks with multitask learning, in: *Proceedings of*

the 25th international conference on Machine learning, ACM, 2008, pp. 160–167.

- [19] D. Ciregan, U. Meier, J. Schmidhuber, Multi-column deep neural networks
505 for image classification, in: Computer Vision and Pattern Recognition (CVPR), 2012 IEEE Conference on, IEEE, 2012, pp. 3642–3649.
- [20] N. Srivastava, G. E. Hinton, A. Krizhevsky, I. Sutskever, R. Salakhutdinov, Dropout: a simple way to prevent neural networks from overfitting., Journal of machine learning research 15 (1) (2014) 1929–1958.
- [21] M. D. Zeiler, R. Fergus, Visualizing and understanding convolutional net-
510 works, in: European conference on computer vision, Springer, 2014, pp. 818–833.
- [22] K. Simonyan, A. Zisserman, Very deep convolutional networks for large-scale image recognition, arXiv preprint arXiv:1409.1556.
- [23] K. He, X. Zhang, S. Ren, J. Sun, Deep residual learning for image recog-
515 nition, in: Proceedings of the IEEE conference on computer vision and pattern recognition, 2016, pp. 770–778.
- [24] Y. A. LeCun, et al., Efficient backprop, in: Neural networks: Tricks of the trade, Springer, 2012, pp. 9–48.
- [25] S. Dieleman, et al., Lasagne: First release. (Aug. 2015). doi:10.5281/
520 zenodo.27878.
URL <http://dx.doi.org/10.5281/zenodo.27878>
- [26] P. et al, Scikit-learn: Machine learning in python, Journal of machine learning research 12 (Oct) (2011) 2825–2830.

- 525 [27] L. Torrey, J. Shavlik, Transfer learning, Handbook of Research on Machine Learning Applications and Trends: Algorithms, Methods, and Techniques 1 (2009) 242.
- [28] S. Lin, Z. Zhao, F. Su, Homemade ts-net for automatic face recognition, in: Proceedings of the 2016 ACM on International Conference on Multimedia Retrieval, ACM, 2016, pp. 135–142.
- 530 [29] J. Margeta, et al., Fine-tuned convolutional neural nets for cardiac mri acquisition plane recognition, Computer Methods in Biomechanics and Biomedical Engineering: Imaging & Visualization 5 (5) (2017) 339–349. arXiv:<https://doi.org/10.1080/21681163.2015.1061448>, doi:10.1080/21681163.2015.1061448.
- 535 URL <https://doi.org/10.1080/21681163.2015.1061448>
- [30] J. Deng, et al., ImageNet: A Large-Scale Hierarchical Image Database, in: CVPR09, 2009.
- [31] V. L. Le, M. Beurton-Aimar, A. Krahenbuhl, N. Parisey, MAELab: a framework to automatize landmark estimation, in: WSCG 2017, Plzen, Czech Republic, 2017.
- 540 URL <https://hal.archives-ouvertes.fr/hal-01571440>

Appendix A. Statistic information on each beetle's part

Table A.9, A.10, A.11, A.12, and A.13 show the statistical values on each
 545 part. The green and red numbers represent the best and the worst values on
 each statistical indicators, respectively.

#LM	Mean	Standard Error	Median	Minimum	Maximum
LM1	2.9914	0.1057	2.7031	0.23	14.2496
LM2	3.4066	0.1306	2.9626	0.175	18.4053
LM3	2.9829	0.1205	2.5864	0.216	19.2092
LM4	3.5449	0.1422	3.117	0.1638	22.8899
LM5	3.3675	0.1327	2.9741	0.101	17.4586
LM6	4.0611	0.1512	3.5733	0.1733	14.0745
LM7	2.9274	0.1159	2.5703	0.2263	14.092
LM8	3.6448	0.145	3.0116	0.1647	15.4585

Table A.9: The statistical values on pronotum images

#LM	Mean	Standard Error	Median	Minimum	Maximum
LM1	4.8185	0.1709	4.2951	0.3732	21.1819
LM2	4.2098	0.1715	3.7484	0.2072	23.9351
LM3	4.7286	0.1705	4.3991	0.2719	19.12
LM4	4.1071	0.1701	3.6232	0.1942	21.6451
LM5	4.1769	0.1545	3.7967	0.2683	20.2307
LM6	3.4976	0.1657	2.9338	0.2384	22.6836
LM7	3.9168	0.1477	3.4284	0.2134	21.0319
LM8	3.402	0.1486	2.7877	0.1478	21.233
LM9	4.1703	0.1481	3.7181	0.4441	22.0267
LM10	3.9433	0.1574	3.4147	0.152	20.7223

Table A.10: The statistical values on head images

#LM	Mean	Standard Error	Median	Minimum	Maximum
LM1	3.2081	0.179	2.6311	0.1265	32.6688
LM2	3.2842	0.1872	2.5934	0.1607	33.9982
LM3	3.1975	0.1755	2.5412	0.0763	31.0928
LM4	3.225	0.1812	2.479	0.1485	33.1458
LM5	3.3062	0.1869	2.606	0.1187	35.7959
LM6	4.2069	0.1957	3.578	0.2149	35.3037
LM7	4.5445	0.2049	4.0792	0.3454	34.7368
LM8	4.7596	0.2018	4.3057	0.4697	32.1749
LM9	4.548	0.1916	3.9626	0.2711	28.3484
LM10	3.3918	0.1772	2.7726	0.1799	29.9211
LM11	3.2897	0.1764	2.7064	0.0527	32.3641

Table A.11: The statistical values on elytra images

#LM	Mean	Standard Error	Median	Minimum	Maximum
LM1	5.2804	0.2805	4.2294	0.6754	41.9898
LM2	4.0548	0.276	3.2748	0.2977	62.6295
LM3	4.013	0.2965	3.0758	0.0416	72.6524
LM4	4.0203	0.2915	3.2101	0.0167	70.5794
LM5	3.9157	0.318	3.1796	0.2025	82.6241
LM6	3.8781	0.3022	3.1983	0.2125	77.8756
LM7	4.0127	0.3306	3.126	0.2276	86.2835
LM8	4.1555	0.3251	3.2471	0.2322	84.0953
LM9	4.349	0.3521	3.3104	0.1464	91.2018
LM10	4.4575	0.3105	3.6117	0.0886	79.3924
LM11	4.7191	0.1915	4.0415	0.4054	27.077
LM12	5.0797	0.2816	4.1478	0.3743	58.941
LM13	4.4999	0.3194	3.5737	0.1282	77.467
LM14	4.2572	0.2776	3.4518	0.4414	66.049
LM15	4.618	0.3165	3.811	0.1256	77.1424
LM16	6.042	0.3312	4.5958	0.1927	62.5569

Table A.12: The statistical values on left mandible images

#LM	Mean	Standard Error	Median	Minimum	Maximum
LM1	4.8759	0.2462	3.721	0.133	26.9596
LM2	4.0644	0.1737	3.3734	0.1778	22.6007
LM3	3.9658	0.1923	3.2037	0.1583	23.8552
LM4	3.8721	0.1823	3.2363	0.0428	21.6248
LM5	4.0479	0.2011	3.1172	0.3983	24.7061
LM6	3.8179	0.1847	3.1692	0.1078	35.2811
LM7	3.7662	0.186	3.0912	0.1559	34.9122
LM8	3.8728	0.1891	3.1345	0.2351	36.0385
LM9	3.9616	0.1948	3.2576	0.1376	35.3078
LM10	3.9661	0.1876	3.3955	0.1709	34.7438
LM11	4.2698	0.1919	3.6016	0.2445	36.3356
LM12	4.4238	0.205	3.7387	0.341	38.4304
LM13	4.8663	0.1922	4.1789	0.3772	27.2213
LM14	4.9318	0.2134	4.0853	0.1473	31.3994
LM15	4.4636	0.1975	3.5378	0.0791	28.7507
LM16	4.1737	0.1838	3.3537	0.3285	25.8165
LM17	4.566	0.1933	3.8441	0.2639	27.9728
LM18	5.8936	0.2812	4.7034	0.1854	30.8248

Table A.13: The statistical values on right mandible images

Appendix B. The distribution of distances on each part

In this section, the distribution of distances on each landmark of each part is shown. The red and green lines are represented for the mean and median values, respectively.

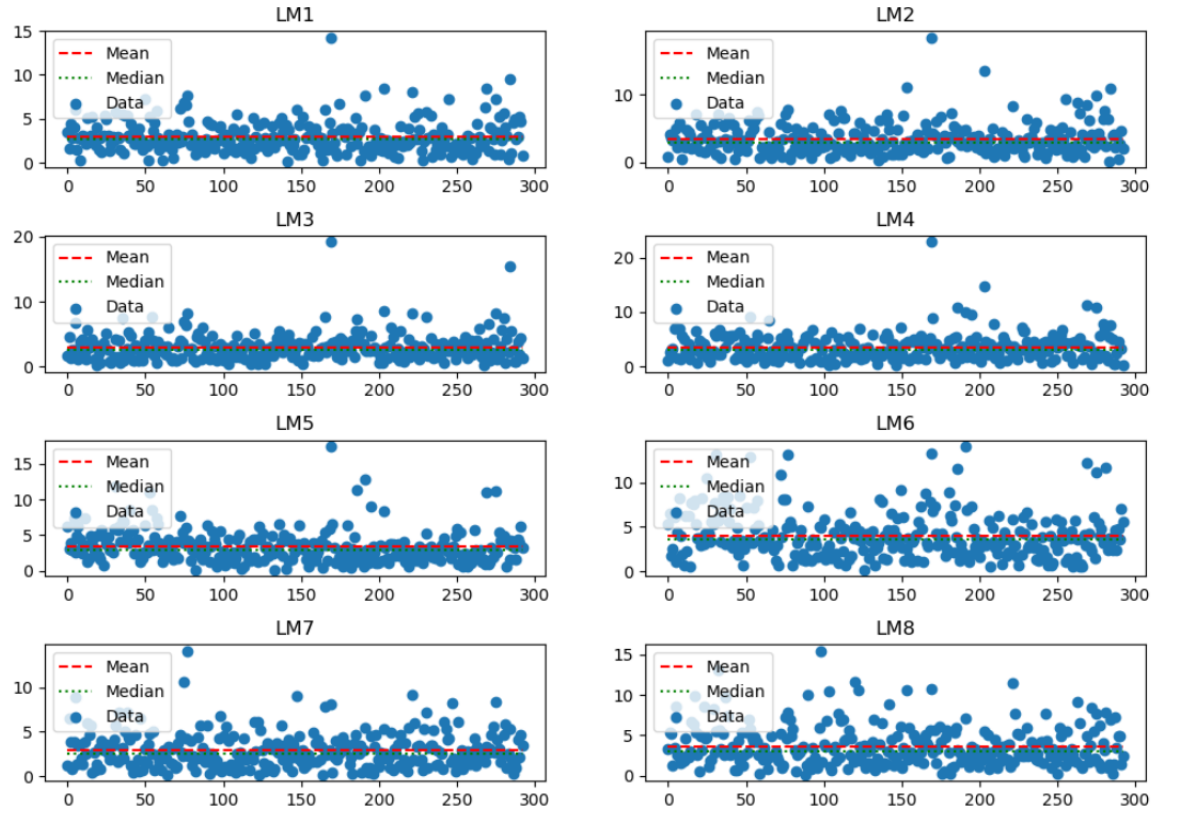


Figure B.14: The distribution of distances on each landmark on pronotum images

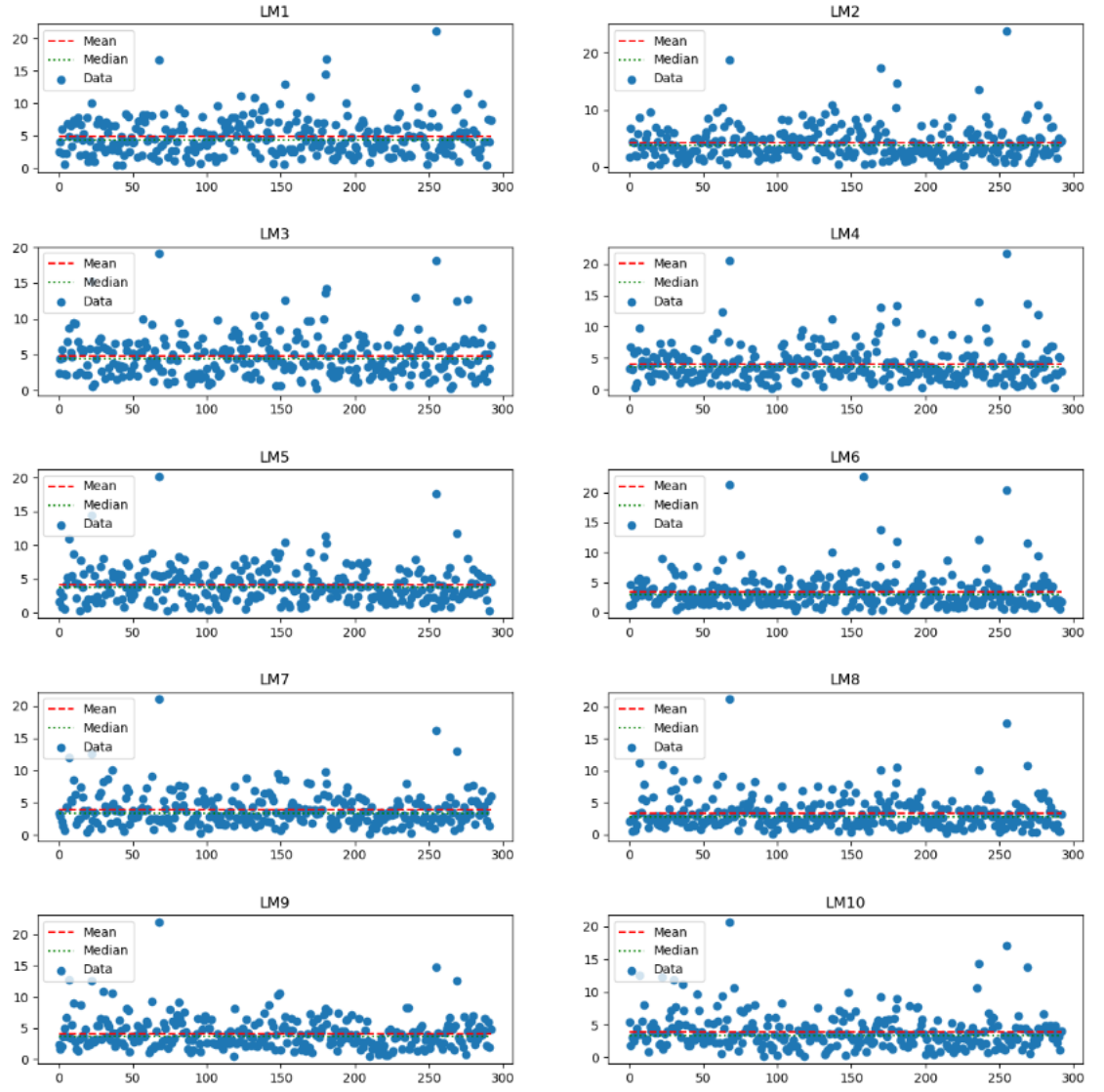


Figure B.15: The distribution of distances on each landmark on head images

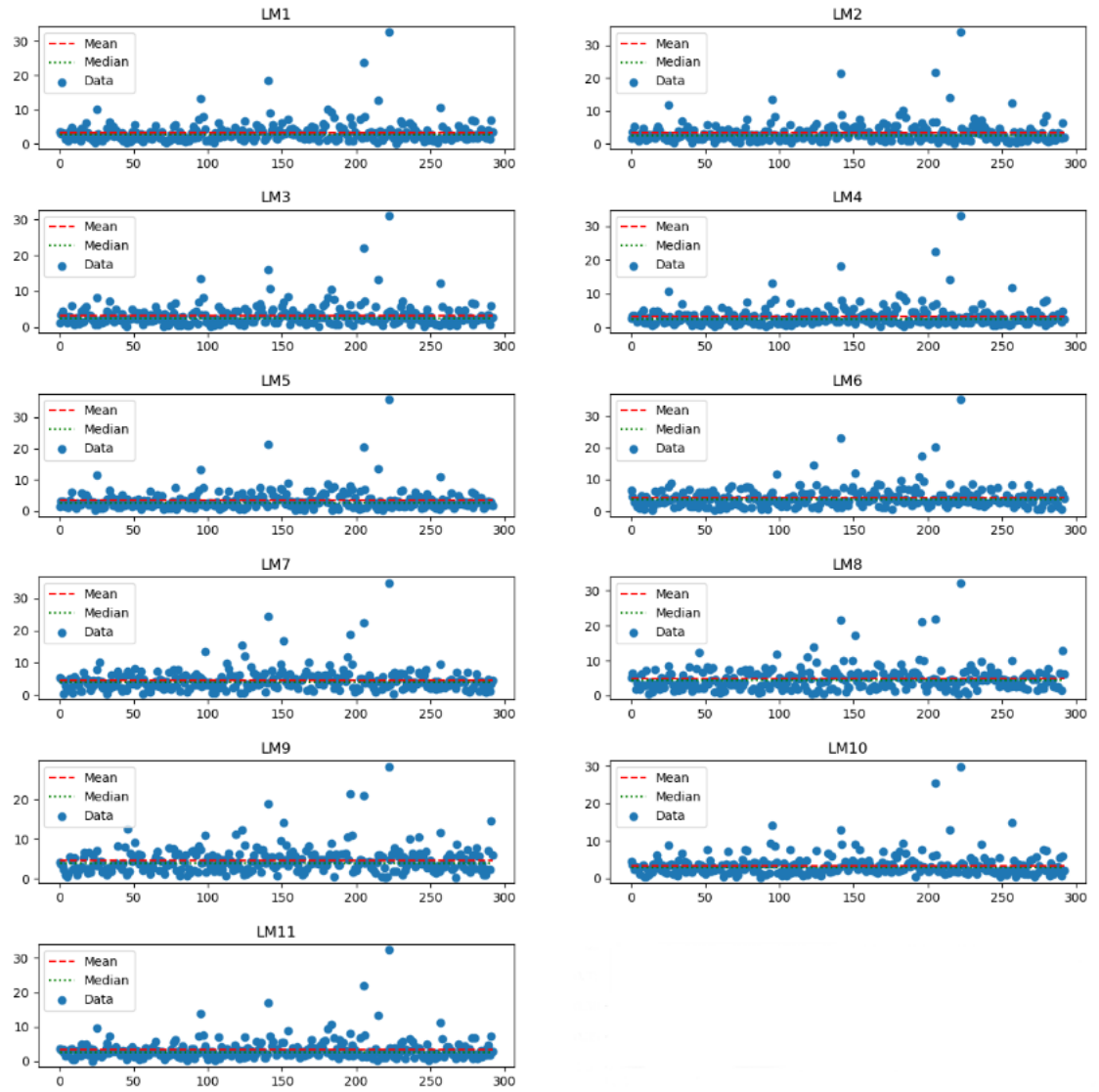


Figure B.16: The distribution of distances on each landmark on elytra images

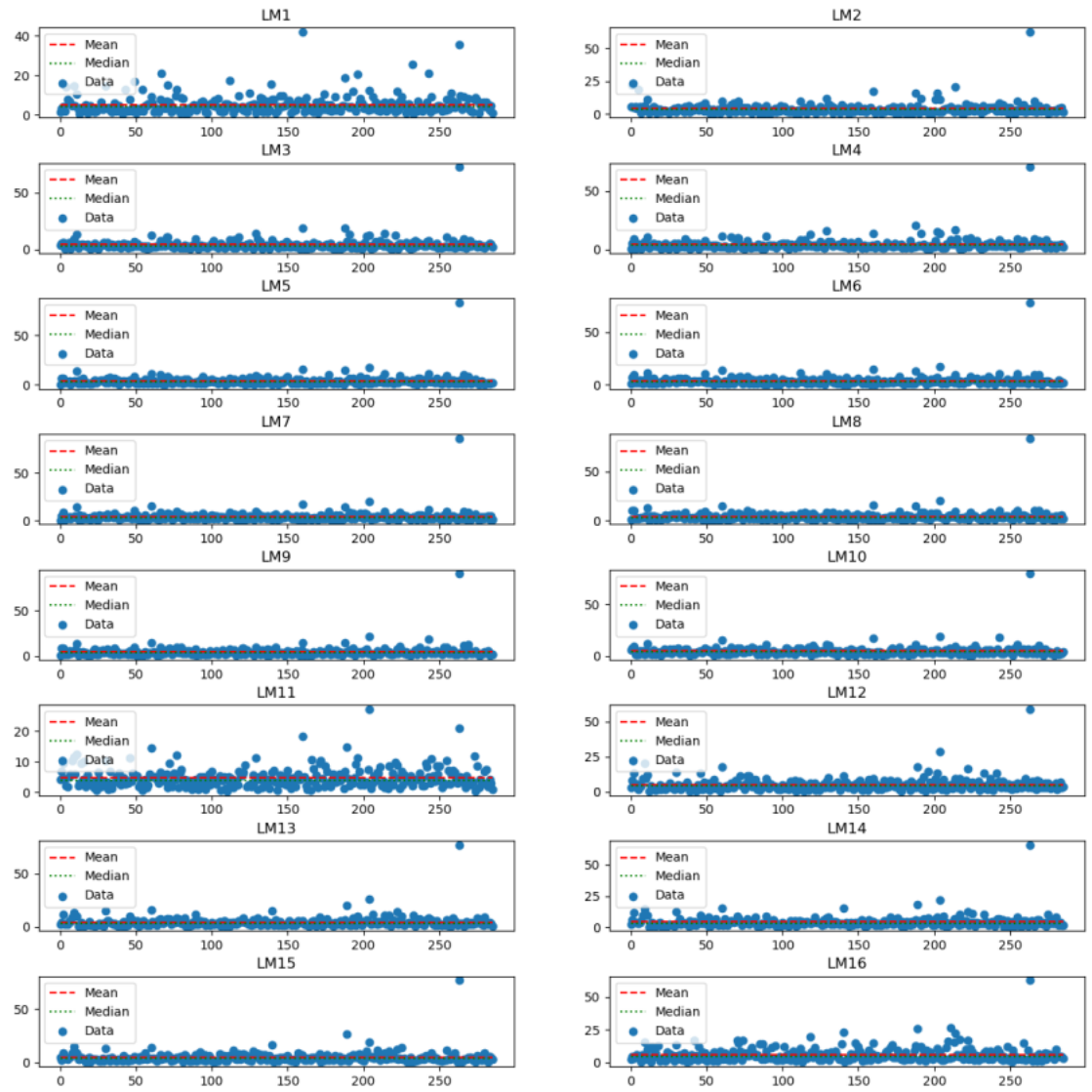


Figure B.17: The distribution of distances on each landmark on left mandible images

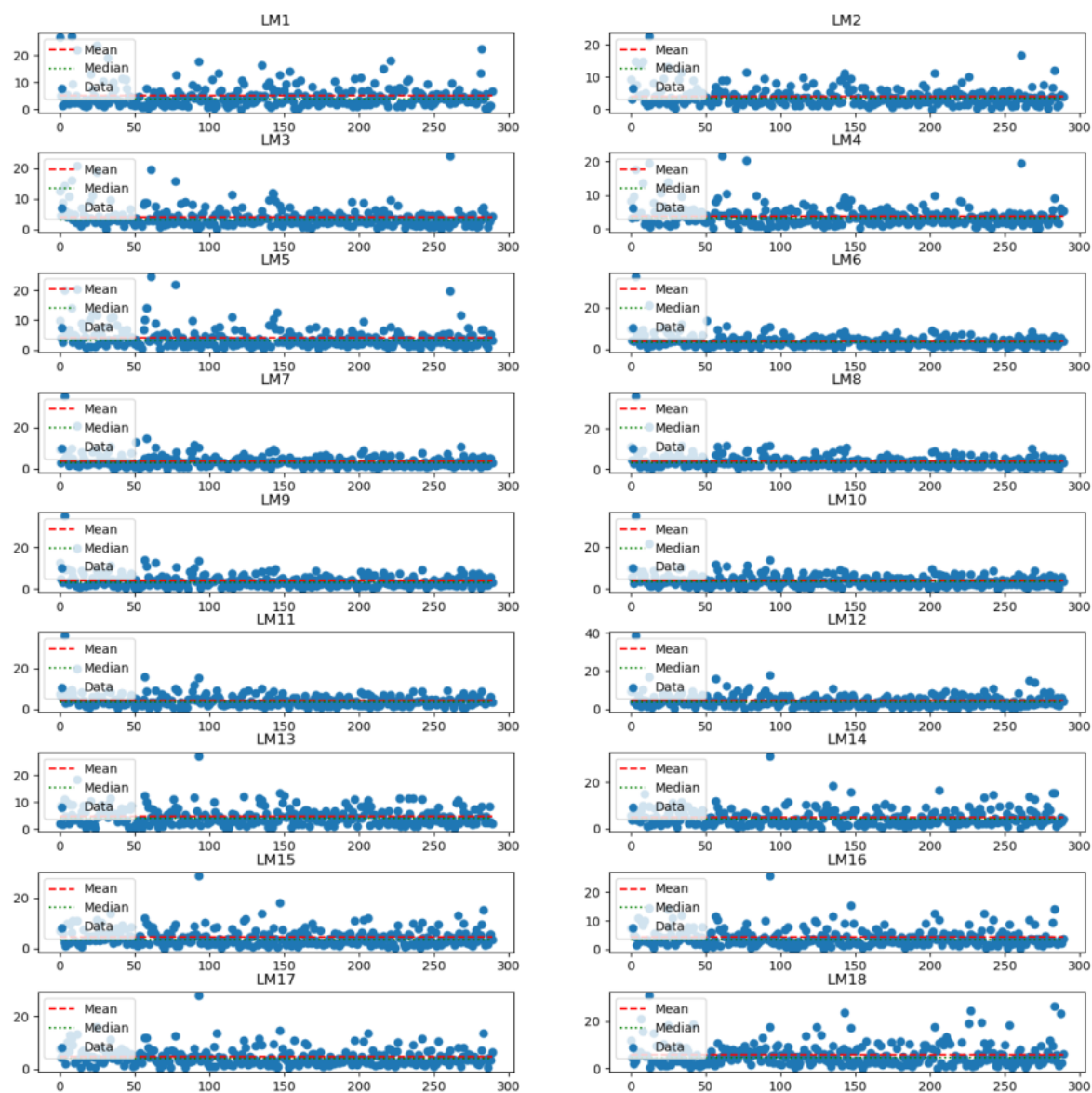


Figure B.18: The distribution of distances on each landmark on right mandible images